

Fundamental limitations of Huygens' metasurfaces for optical beam shaping

Carlo Gigli¹, Qitong Li², Pierre Chavel³, Giuseppe Leo¹, Mark Brongersma², Philippe Lalanne^{4}*

¹ Matériaux et Phénomènes Quantiques, Université de Paris & CNRS, 10 rue A. Domon et L. Duquet, 75013 Paris, France

² Department of Materials Science and Engineering, and Geballe Laboratory for Advanced Materials, Stanford University, Stanford, California 94305, USA

³ Laboratoire Hubert Curien, Université de Lyon, Univ. Jean Monnet de Saint Etienne, Institut d'Optique Graduate School, CNRS UMR 5516, 42000 Saint Etienne, France

⁴ Laboratoire Photonique, Numérique et Nanosciences (LP2N), Institut d'Optique Graduate School, Univ. Bordeaux, CNRS, 33400 Talence Cedex, France.

*Corresponding author: Philippe.lalanne@institutoptique.fr

Keywords: Huygens' metasurfaces, wavefront control, subwavelength metasurfaces, beam shaping

High-index optical metasurfaces composed of arrayed nanostructures are expected to enable arbitrary spatial control of incident wavefronts with subwavelength spatial resolution. For phase modulation, one often resorts to either of two physical effects to implement a 2π -phase excursion. The first effect relies on waveguiding by nanoscale pillars and the second one exploits resonant confinement by high-index nanostructures with two degenerate Mie-resonances. We compare the two approaches and identify fundamental limitations with the latter, known as Huygens' metasurfaces. Based on numerical evidence, we explain the reasons for the weak diffraction efficiencies of recently reported dielectric Huygens' metasurfaces. We conclude by providing several very general and intuitively understandable arguments that suggest that imprinting rapid spatial phase variations to an incident wavefront with nanoscale resonators is not a generally viable approach.

1. Introduction

In integrated circuits, an important prerequisite for success is that every transistor or memory element can be driven or read independently, and nanotechnology is used to push the integration limit subject to that essential requirement. In dielectric metasurfaces for wavefront shaping, one

aims to imprint spatially varying phases (or amplitudes, polarizations) on an incoming optical beam, and nanotechnology is used to spatially control the phase down to the subwavelength scale, as required for high numerical aperture focusing or imaging, beam steering over large angles, and computer-generated holography. Just like for integrated circuits, it is important that the phase can independently be controlled by adjacent nanostructures (or meta-atoms). This demanding requirement has marked the history of diffractive optics and has led to the emergence of two families of metasurfaces: optical phased-array antennas ^[1] and Huygens' metasurfaces ^[2].

Both these denominations are confusing since they support the same idea of harnessing the phase at the subwavelength scale. In fact, more precisely, these device families are strictly associated to two different mechanisms: guidance along nanoscale pillars implementing wavefront phase differences ^[1,3] and nanoconfinement combining two resonances, each covering a standard phase range of π ^[2,4,5]. Many good reviews exist on the topic ^[6-11]. Note that exactly the same mechanisms have also been used to control the geometrical phase ^[12-14]. Geometric-phase control will not be analyzed hereafter; however, we expect that the following conclusions remain qualitatively valid.

Guidance along nanopillars has long been known to provide high diffraction efficiencies (~80% routinely) at large deviation angles ^[1,3,14], be tolerant to changes of illumination directions ^[15], and is presently attracting renewed interest ^[9,10,12,14,16-18]. These important properties result from a waveguiding effect ^[19], which makes the nanopillars behave “as nearly-independent coherent emitters and the blazed binary element as a phased-array antenna operating in the optical domain” (to quote Ref. ^[1]).

The resonant mechanism is much more recent ^[2,4,5,12] and is well understood from a simple picture where every nanoresonator can provide an electric and a magnetic dipolar resonance ^[2,20] with opposite phases to achieve forward scattering ^[21]. Together, these resonances make

each nanoresonator behave as a secondary source that emits “purely forward-propagating elementary waves, as required by the Huygens’ principle” (Ref. [2]).

Importantly, Huygens’ metasurfaces require much smaller aspect ratios than nanowaveguide metasurfaces, and thus are more readily amenable to low-cost large-scale manufacturing. Owing to this promise and their reputation of excellent performance, they are also drawing a strong attention [22–27].

In this work, we put forward the idea that, despite their strong reputation, Huygens’ metasurfaces applied to wavefront shaping suffer from a fundamental limitation at optical frequencies: the difficulty (or impossibility?) to implement arrays of resonant forward-scattering meta-atoms that are spaced at submicron distances and still control the phase independently. Although the literature has already evoked limitations of the Huygens’ approach [4,10,25,27,28] and has even tried to overcome some of them through global optimization [25,27], we think that, as a community, we have been underappreciating the importance of these limitations and overlooking their fundamental character.

In a first step, we aim to show how critical the limitations are. This will be evidenced by a numerical study of the performance of the pioneering Huygens’ design reported in [2]. We show that the efficiency of these elements remains below 40%, even for large metagratings with periods significantly larger than the wavelength for which classical low-cost sawtooth diffractive optical elements show excellent performance, around 90%. We explain the low performance by a shadowing effect due to optical coupling between adjacent metaatoms.

In a second step, we briefly review recent efforts to improve the Huygens’ metasurface performance, essentially by global optimization of the feature sizes and locations of the metaatom features through electromagnetic computations. Significant improvements have been reported theoretically in some cases, but the experimental results remain inferior to those of sawtooth diffractive optical elements. A global optimization, at the scale of one or several periods, synchronizes the scattering of an ensemble of elements towards a specific goal. In no

way, it may result in an individual control of the phase at the subwavelength scale. The reverse is the case.

Clearly, all the promised benefits of nanotechnology are not gathered in Huygens' metasurface. But this conclusion is so-far based on observations made for specific geometries (the initial Huygens' design analyzed in the first step or optimizations performed by other researchers summarized in the second step). In the third step, we provide general arguments for the drawbacks of the Huygens' approach. Our arguments rely on very general concepts, e.g. cross-sections, crosstalk, number of modes, symmetry breaking and lead to general conclusions about the fundamental limitations announced in the title.

We emphasize again that our discussion holds for *beam-shaping applications requiring a subwavelength control of some wave features* (phase, amplitude, polarization) and for operation in the visible domain with dielectrics. At longer wavelength domains, for which materials and technologies are different, our general conclusions are still worth considering in our opinion, although different conclusions might apply.

2. Numerical evidence for a testbed case

In this Section, we consider the initial Huygens' design reported in ^[2], based on Si nanodisks embedded in a homogenous medium ($n_h = 1.66$) (Figure 1b). We compute the diffraction efficiency for a series of metagratings with decreasing periods, to test the design capability to encode phase profiles that are gradually varying at increasing rates. For the sake of illustration, we compare the results with those achieved for TiO₂ square-based nanoposts on a SiO₂ substrate (Figure 1a), a geometry that exactly corresponds to the optical phasar proposed in ^[3]. The performance of such an approach has been duly published ^[1,3,8,15] and is used as a reference. The initial design of any metasurface often relies on the creation of an abacus (or lookup table) which provides a systematic, one-to-one mapping between the desired phase profile and the required meta-atoms ^[2,3]. An abacus is crucial as it can be computed very quickly and offers an

initial guess for the ideal choice of meta-atom, which may then facilitate rapid prototyping or further computationally-demanding global optimizations. They are usually computed by considering periodic arrays of identical meta-atoms illuminated at normal incidence and by extracting the phase of the transmitted zeroth-order as a function of some tuning parameters, in general the meta-atom size or shape. Let us note that this natural approach is optimal at least for metasurfaces encoding phase increments significantly smaller than $2\pi/\lambda$ between two successive elements. However, for rapidly varying phases, the neighboring meta-atoms of functional metasurfaces are all quite different and the abacus based on an artificial periodization cease to be strictly valid. In addition, the computation being performed at normal incidence, the abacus includes some symmetries that are lost in the functional metasurfaces. These remarks will help us in the following to understand why abaci are not always helpful to evaluate the performance of functional metasurfaces, in particular for Huygens' metasurfaces.

The following computations are performed with the rigorous coupled-wave analysis (RCWA) implemented with the RETICOLO freeware ^[29], occasionally improved with the advanced solver reported in ^[30], and with COMSOL Multiphysics. The results have been cross-checked. We first compute the abacus to create a library of elements providing a continuous phase shift across the $[0, 2\pi]$ range. Let the constitutive "meta-atoms" be arrayed in 2D square lattices, and the abacus be obtained by computing the (0,0)th-order transmission coefficients for a normally-incident plane wave at a fixed vacuum wavelength λ , by tuning the dimensions of the constitutive meta-atoms while keeping constant the unit cell size A .

The abaci of the Huygens and phasar approaches are reported in Figure 1. They are obtained by computing the (0,0)th-order transmission coefficients for a normally-incident plane wave at a fixed vacuum wavelength λ , by tuning the dimensions of the constitutive meta-atoms while keeping constant the unit cell size A . Please note that due to the symmetry of the systems these results are valid for both polarizations along the x and y axes. The abacus is consistent with

previous data in ^[3] and ^[2], evidencing a near-unity transmission for the required 2π phase excursion.

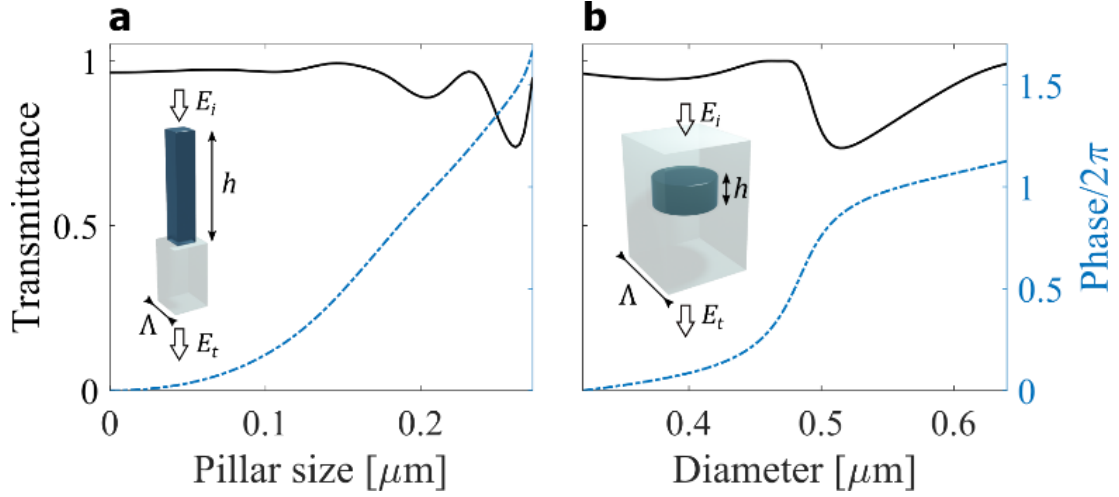


Figure 1. Abacus of the zero-order transmission coefficient of gratings formed by identical meta-atoms organized in a square lattice of periodicity Λ . **(a)** Geometry in ^[3], with TiO_2 ($n_{\text{TiO}_2} = 2.3$) nanopillars with square basis on a SiO_2 substrate ($n_s = 1.46$). $\Lambda = 272$ nm and $\lambda = 633$ nm. **(b)** Geometry in ^[2], with Si ($n_{\text{Si}} = 3.5$) nanodisks embedded in a host medium ($n_h = 1.66$). $\Lambda = 666$ nm and $\lambda = 1340$ nm. A plane wave normally-incident on the grating from the upper layer (air for the TiO_2 nanopillars) and linearly polarized along the x -axis is considered in both cases. 17×17 Fourier coefficients are retained for the numerical computation with the RCWA.

The abaci are then used to design two series of blazed gratings with increasing periods, each impressing the same sawtooth phase profile. The gratings with the smallest period $a = 3\Lambda$ contain three meta-atoms. The periods are then increased step by step up to $a = 10\Lambda$. The design procedure is exactly the same for the two platforms. For metasurfaces with N meta-atoms per period, the disk diameters and pillar sizes are chosen from the abaci to implement a

phase profile $\varphi(x_p) = \frac{\pi}{N} + \frac{p2\pi}{N}$ with x_p the position of p^{th} element and $p \in [0, 1, \dots, N - 1]$.

The procedure is detailed in [3].

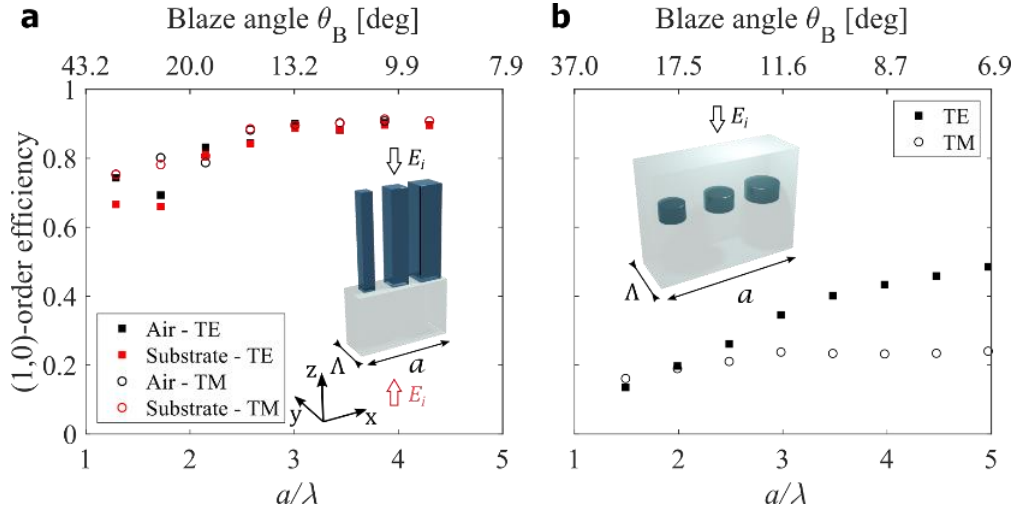


Figure 2. Comparison between the theoretical performances of meta-gratings designed with the abacus described in Figure 1 to be blazed into the (1,0) order. The unitary cell dimensions of the meta-gratings are $N\Lambda = a$ along the x -axis and Λ along the y -axis, where N is the number of meta-atoms in the super cell. (a) Constitutive meta-atoms are TiO₂ nanopillars with square basis ($\Lambda = 272$ nm, $\lambda = 633$ nm). (b) Constitutive meta-atoms are Si nanodisks ($\Lambda = 666$ nm, $\lambda = 1340$ nm). The results are obtained for plane waves, polarized along either the y (TE) or the x (TM) axis and normally incident from either the substrate or the superstrate (the four cases are represented with different colors or signs). Due to the system symmetry substrate and superstrate incidence results are identical in (b). The number of Fourier components retained in the RCWA computation is $(N \times (2MM + 1), (2MM + 1))$ along the (x, y) directions with $MM = 8$. In (a), the blaze angle is in the substrate.

The results obtained in Figure 2 for the TiO₂ metagratings are consistent with earlier works [1,3].

At large periods, the first-order efficiency reaches a plateau; all the transmitted light feeds the

first order, the missing energy being reflected due to an impedance mismatch. The efficiency decrease for small period-to-wavelength ratios mainly results from an under-sampling of the phase, only three waveguiding nanoposts being used for the smallest period.

In sharp contrast, a much weaker performance is obtained with Huygens' nanodisks. The missing energy feeds all transmitted and reflected orders, therein implying that neither a phase gradient nor the Kerker condition are achieved. A quantitative analysis demonstrating how the Kerker condition is broken in meta-gratings is provided in Supplementary Section S1.

Thus, the initial design proposed in ^[2,4,5] with Si nanodisks does not meet our expectation in terms of efficiency, even for low deviation angles for which alternate sawtooth diffractive elements provide large efficiencies at lower fabrication costs. We have verified, with numerical results not reported here, that similar conclusions also hold for more elaborate Huygens' metasurfaces recently designed with quadrupoles (instead of dipoles) ^[22]. We are also forced to conclude that the abacus computed for uniform arrays of identical meta-atoms are, in general, not reliable indicators of the performance of functionalized metasurfaces implementing graded variations, even when the spatial gradients are small compared to the wavenumber.

3. Explanation for the low performance observed for the testbed case

3.1. 'The Shadowing effect'

To understand the reason for the low performance, Figs. 3(a-c) compare the near-field maps of nanodisks with different diameters, all for the same wavelength, TE-polarization and incident angle $\theta_i = 0^\circ$ (a-b) or $\theta_i = -4.3^\circ$ (c). Sixteen nanodisks are considered. They are isolated in Figure 3(a) or arrayed in (b-c) exactly as for the computation of the Huygens' abacus of Figure 1(b). The diameters are chosen to uniformly sample the $[0, 2\pi]$ phase interval. The near-field maps are all plotted with the same color scale. They are significantly different, therein evidencing that the arrayed nanodisks are electromagnetically coupled and do not behave as independent entities.

Figure 3(d) shows the actual near-field of a meta-grating supercell composed by associating the 16 nanodisks in a row. The total period $a \approx 10.66 \mu\text{m}$ corresponds to a first-order deviation angle of 4.3° ; the metagrating efficiency is 60% for TE-polarization. A direct visual inspection evidences that the near-field maps in (b) and (d) largely differ, the more spectacular contrast occurring for the nanodisks on the right and left sides of the period close to the 2π phase jump. The jump forces the association of small and large nanodisks and thus strongly breaks the translational invariance used for the abacus computation. That explains why the abacus field maps are not recovered for the outermost nanodisks neighboring the jump, in a $\approx 4\lambda$ -wide “transient zone” corresponding to a total of 8 pillars (4 on each side of the jump). Just like the shadow zone effect occurring in conventional sawtooth diffractive optical elements ^[1], this zone considerably reduces the efficiency of Huygens’ meta-gratings.

We have also studied the near-field maps of TiO_2 pillars. Consistently with ^[1,19], we find that all the maps are quantitatively the same: the arrayed TiO_2 pillars behave almost independently from each other.

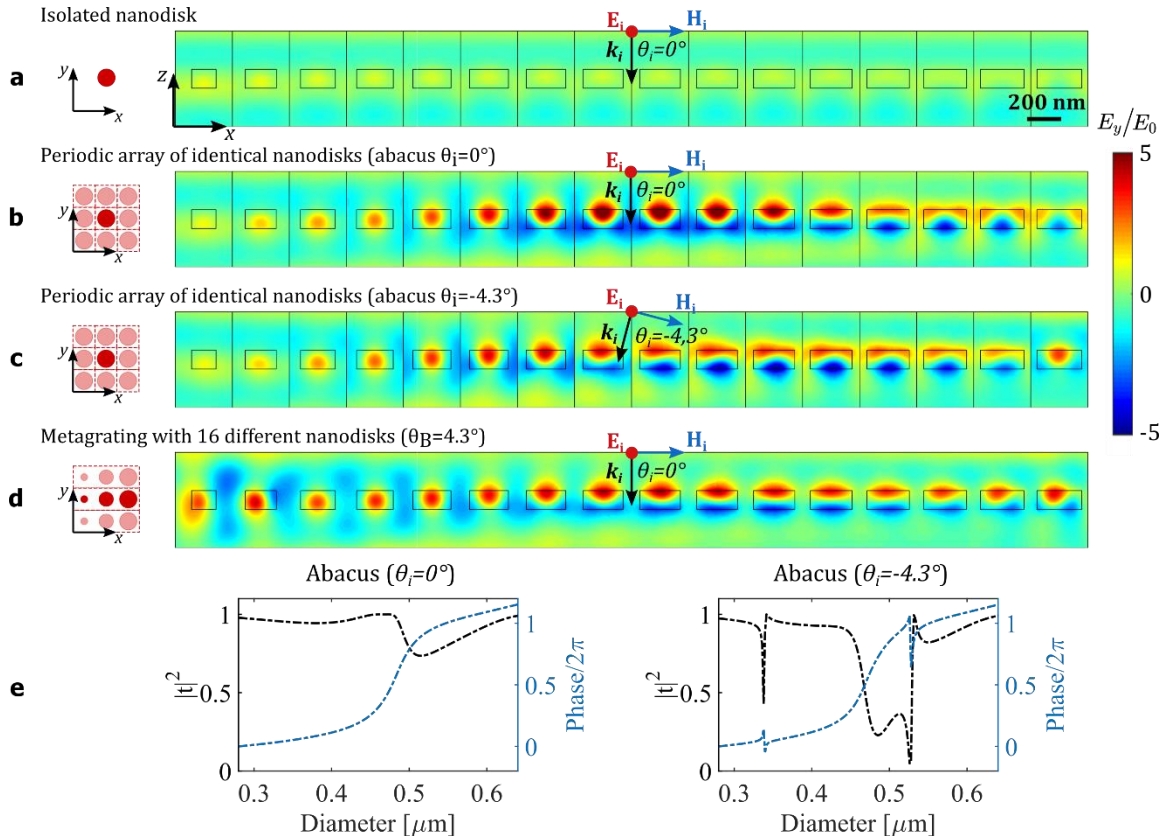


Figure 3. Analysis of the y -component of electric near-field maps in the xz plane of Huygens' meta-gratings. All the maps are obtained for the same polarization (TE) and wavelength ($\lambda = 1340$ nm). Incident electric/magnetic field orientations are reported with red/blue arrows. Field amplitudes are normalized to the incident field. **(a)** Isolated nanodisks. **(b)** Arrayed nanodisks like in the abacus of the right panel in Figure 1. The diameters are chosen to uniformly sample the $[0, 2\pi]$ phase interval. **(c)** Same as in (b) but for an incidence of $\theta_i = -4.3^\circ$, which corresponds to the deviation angle into the first transmitted order of the meta-gratings in (d). **(d)** Supercell composed by associating the 16 meta-atoms in a row designed for a deviation angle $\theta_B = 4.3^\circ$. **(e)** Transmission coefficient comparison, in square modulus (black) and phase (blue), between a beam impinging at $\theta_i = 0$ (left) and $\theta_i = -4.3^\circ$ (right) on a uniform metasurface of identical nanodisks. The same color scale is applied in all plots, allowing for a direct comparison. A similar figure for the other polarization can be found in the SI.

3.2. Symmetry breaking: the hidden modes

After focusing our attention on the outermost 8 nanodisks, let us further consider the near-field maps of the 8 nanodisks of the central zone in Fig 3d. Owing to the progressive variation in disk diameters (the diameter d only changes by 5 nm on average between adjacent disks), one expects the maps to more closely resemble the abacus maps in Figure 3b. Although the resemblance is better than for the nanodisks in the transient zone, it is far from perfect (consider the field at the nanodisk rear interfaces), especially in view of the minute changes in diameter, $\Delta d/d \approx 5\%$, between adjacent pillars.

To explain the hypersensitivity of the metasurface even for *gradual* and *tiny* variations, one may argue that the nanodisks collectively behave as resonators. Although reasonably valid, this argument alone does not appear sufficient. A symmetry argument should be added.

Symmetry breaking has surprising consequences in many fields, even with infinitesimally tiny modifications. In the present context, it is the discrete translational symmetry (i.e. periodicity) of the abacus geometry that is broken in Huygens' meta-gratings. This results in a stringent asymmetry in the near-field maps of Figure 3d for the disks in the transient zone. The asymmetry is also visible in the central zone upon close examination of the blue and red areas on the rear and front side of the disks.

To evidence the origin of the asymmetry, we have computed the Bloch modes for all the disk diameters of the abacus for normal incidence. Up to six modes are found for large disks, three being symmetric and the others antisymmetric (with respect to the vertical plane). Their effective indices (normalized propagation constant along the z-axis) are shown in Figure 4a and their transverse field maps for a disk diameter of 550 nm in Figure 4b. Indeed, only the symmetric Bloch modes contribute to the maps of the abacus of Figure 3(e) at $\theta_i = 0$. However, all modes, symmetric or antisymmetric, play an important role in meta-gratings with a large period (i.e. with slowly varying phase gradients), even at normal incidence.

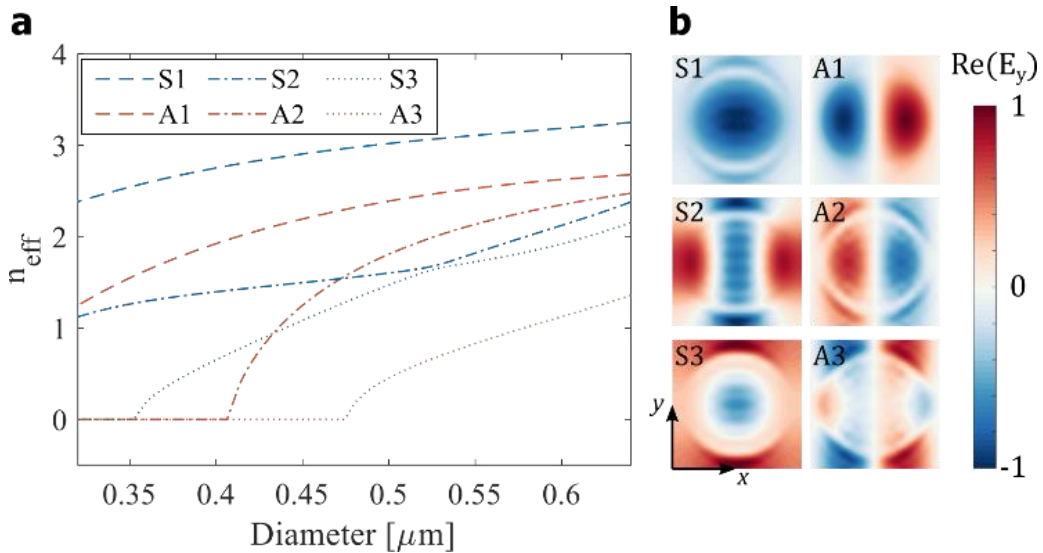


Figure 4. Bloch modes of periodic arrays made of identical Si nanodisks embedded in a host medium ($n_h = 1.66$) for $\Lambda = 666$ nm and $\lambda = 1340$ nm. (a) Effective

index of the six non-evanescent Bloch modes. **(b)** Real part of the electric field y -component for the same six Bloch modes in case of nanodisks with diameter $d = 550$ nm.

To fully realize why, consider a meta-grating designed to be blazed into the first transmitted order upon illumination by a normally-incident plane wave. The same grating back-illuminated from the first transmitted order on the rear side, will diffract light normally with the same efficiency. Now, owing to reciprocity, we clearly realize that a proper design cannot rely on computational data involving only symmetric Bloch modes ^[31].

Figure 3(c) shows the near-field maps of the 16 nanodisks, computed this time for an incidence angle $\theta_i = -4.3^\circ$, which corresponds to the deviation angle of the metagrating first order in Figure 3d. In Figure 3e, we further show the phase and the (0,0) transmitted intensity. Clearly the antisymmetric modes have a strong impact ^[8]: despite the small $\Delta k_{//}$ values, the maps in (b) and (c) are completely different. The transmittance reported in Figure 3e displays deep dips, which are strongly polarization dependent (not shown), considerably reduce the efficiency and preclude a fine control of the imprinted phase. Experimental demonstrations of Huygens metasurfaces sensitivity to incidence angle have been reported in ^[32].

4. Optimization of Huygens' metasurfaces: an overview of recent results

The weak efficiencies reported in Figure 2b are consistent with experimental results based on abacus designs. In ^[5], metaatoms etched in polycrystalline silicon are used to steer at 14° a laser beam at 1550 nm with a measured efficiency of 36%. In ^[4], an efficiency of 45% is measured for a metagrating that diffracts a laser beam at 705 nm by 10° . Similar performance is reported in ^[26] for a metagrating operating at 650 nm with a 36% efficiency.

To enhance the efficiency, it is necessary to compensate for the electromagnetic-coupling variations that occur in spatially variant diffractive elements and are not accounted for in the

abacus based on translation invariance. In ^[28], the authors propose to mitigate the impact of the coupling variation between nearest neighbors with a supercell approach based on the repetition of four identical Si nanodisk metaatoms. The approach that clearly reduces fine-sampling capabilities has been tested for a hologram operating at 785 nm and did not really provide a performance improvement in terms of efficiency with a measured efficiency of 24%.

Instead of trying to avoid or minimize the interactions among meta-atoms, one may rather consider and resort to global optimization by locally adjusting the metaatoms morphology initially designed with the abacus. A few examples are reported in the literature. In ^[25], the performance of a metagrating has been optimized by slightly changing the size and position of the nine Si nanodisks arrayed to form the grating period. An experimental efficiency of 57% in the first order (10° deviation) has been measured for normal incidence and for the designed linear polarization at 1340 nm (a large efficiency drop is reported for the other polarization). Another example is found in ^[27], in which global optimization of hundreds of TiO₂ nanodisks have been performed with a genetic algorithm and cylindrical lenses of a few tens of microns in diameters were fabricated with a high-precision fabrication process for green light ($\lambda = 532$ nm) operation. Compared to conventional designs based on abacus, significant performance improvement has been demonstrated. For instance, a 24- μ m-diameter lens with a 60% efficiency and a 0.51 NA has been manufactured. Note that this interesting result holds for normally-incident light and linearly polarized light like in the previous example. Further note that cylindrical lenses, like metagratings, are translational variant only in one direction and that a full control of the coupling variations is not required.

These performances, albeit largely improved compared to classical abacus design, do not in our opinion suggest that Huygens' metasurfaces are a promising approach to wavefront shaping. They are lower than those achieved with the nanowaveguide approach for similar devices, see ^[1,3,9,10,12,14,16–18,33]. They are also lower than the performance achieved with optimized multilevel profiles, see for instance ^[34]. Inverse design with optimization always increases the performance.

However, the approach requires a good initial guess and is computationally intense, especially for non-periodic metasurfaces to perform functions like hologram generation. When global optimization results in a strong performance increase, the result is often highly angle and wavelength sensitive ^[25,27]. This is a consequence of the non-local behavior and we emphasize that such global optimization does not contribute in any way to a subwavelength scale control of the phase. On the contrary, it favors a macroscopic collective behavior. In our opinion, the substantial role played by non-local interactions in Huygens' metasurfaces prevents a nice conceptual paradigm that leads to metaatoms operating independently like in integrated circuits.

5. General arguments on the limitation of resonant approaches

The essence of the Huygens' flat-optics can be traced back to a series of pioneering works on individual resonant nanoparticles that scatter forward ^[20,21,35,36] and to the idea of arraying these nanoparticles to locally monitor the phase. A Huygens' component is thus an optical phased-array antenna composed of *resonant* metaatoms that should independently scatter forward with a prescribed phase.

As we have seen, the initial design with Si nanodisks abacus has a limited scope and refinements through global optimization do not fundamentally change the situation. The question arises if one faces fundamental limitations. Several general arguments suggest that imprinting rapid spatial phase variations to an incident wavefront with nanoresonances is not a viable approach.

Resonance is incompatible with fine sampling. On resonance, the extinction cross-section of every individual metaatom is significantly larger than its geometrical cross section and every metaatom thus acts as a funnel that broadly summons the incident field. Safe operation requires the interelement separation distance to be typically equal to the cross-section, as sketched in Figure 5a, implying that fine samplings of the phase (polarization ...) cannot be implemented. Comparatively, the nanopillar approach is antiresonant. For high index semiconductor materials

that may reduce aspect-ratio requirements, the pillar facets become reflective, the nanopillars start to behave as resonators, and the performance drops. Facet anti-reflection coatings are then necessary ^[37].

Resonance favors crosstalk. A consequence of the funnel effect is the field enhancement in the resonator on resonance. Even in the favorable assumption that metaatom coupling occurs through evanescent fields, the enhancement is indeed felt by neighboring metaatoms, implying that the stronger the resonance, the larger the crosstalk, see Figure 5b. The same limitation holds for the nanowaveguide approach, but comparatively, since the approach is essentially nonresonant, the relative weight of the incident field in the actual total field driving the metaatoms is stronger and thus the possibility to spatially control the phase down to the subwavelength scale is reinforced. Note that, in the Huygens approach, inherently, crosstalk does not result from evanescent waves but from progressive ones, and this reinforces the crosstalk as we argue now.

Dipolar resonances promote long range interactions. For tiny particles of size b , the magnetic-dipole radiation power is by a factor $(kb)^2$ smaller than the electric-dipole radiation power, and therefore forward scattering with thin elements requires the embodiment of resonators with a multipolar nature. These resonators, which operate far away from the static electric-dipole approximation, scatter progressive waves, enabling crosstalk between even distant metaatoms as shown in Figure 5c. The issue is reminiscent of the work on negative-index optical materials, for which one should ideally design arrays of independent meta-atoms supporting magnetic resonances. At optical frequencies, the best negative index material, the fishnet ^[38], implements negative refraction through a transverse resonance that involves an array of four meta-atoms when metal loss is considered, and a few tens of meta-atoms when loss is compensated ^[39]. Like in the present work, advanced and strong resonances boost long range

crosstalk and prevent independent operation. For the nanowaveguiding approach, the coupling is essentially short range, through the evanescent field of the nanopillar guided modes. We further note that, for ultra-flat reflecting metasurfaces operating with a single electric-dipolar resonance only, better performance is achieved ^[40].

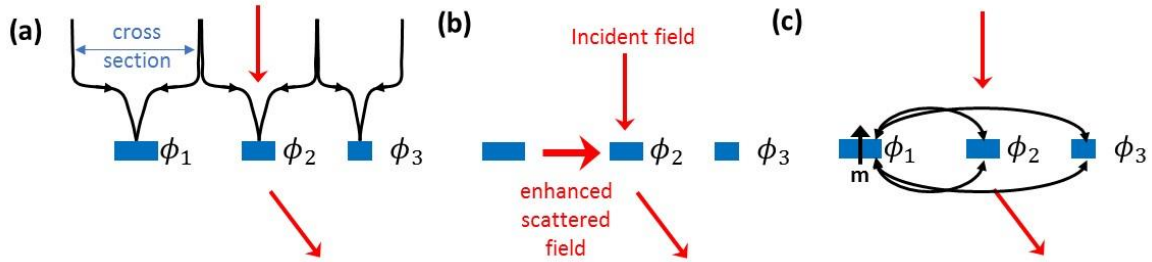


Figure 5. (a) Resonant funneling imposes a large separation distance (\sim extinction cross section) between the metaatoms and thus prevents fine sampling. (b) The actual driving field is the sum of the incident field and the field scattered by neighbors. The stronger the resonance, the weaker the incident field contribution and the lesser the possibility to locally monitor the incident field. (c) Strong magnetic dipole resonance, with a magnitude comparable to electric ones, favors long range crosstalk with progressive waves.

6. Conclusion

The comparison of the principles of operation of nanowaveguide phased-array antennas and ultra-flat Huygens' metasurfaces shows that the former remains the simpler and more efficient way to imprint rapidly varying phases at optical frequencies. Provided that the waveguide spacing is suitably chosen ^[1], neither too small to avoid the homogenization regime, nor too large to remain below the structural cutoff for which second-order progressive Bloch modes appear, good performance is obtained at the design frequency.

Although alternative designs maintaining all the benefits of ultra-flat nanostructured elements are not strictly ruled out by our analysis, we believe that the fundamental limitations we bring

up in Section 5 should be considered before tackling the design challenge. We wish that pointing out the different facets of the challenge will help circumvent the current limitations.

Funding sources and acknowledgments

PL and GL acknowledge NOMOS Project (ANR-18CE24-0026) for financial support. MLB and QL are funded by individual investigator grants from the department of energy (Grant DE-FG07-ER46426) and Airforce (Grant FA9550-18-1-0323).

Acknowledgments

GL thanks Giuseppe Marino for fruitful discussions.

References

- [1] M. S. L. Lee, P. Lalanne, J. C. Rodier, P. Chavel, E. Cambril, and Y. Chen, *J. Opt. A Pure Appl. Opt.* **4**, S119–S124 (2002).
- [2] M. Decker, I. Staude, M. Falkner, J. Dominguez, D. N. Neshev, I. Brener, T. Pertsch, and Y. S. Kivshar, *Adv. Opt. Mater.* **3**, 813–820 (2015).
- [3] P. Lalanne, S. Astilean, P. Chavel, E. Cambril, and H. Launois, *J. Opt. Soc. Am. A* **16**, 1143–1156 (1999).
- [4] Y. F. Yu, A. Y. Zhu, R. Paniagua-Domínguez, Y. H. Fu, B. Luk'yanchuk, and A. I. Kuznetsov, *Laser Photonics Rev.* **9**, 412–418 (2015).
- [5] M. I. Shalaev, J. Sun, A. Tsukernik, A. Pandey, K. Nikolskiy, and N. M. Litchinitser, *Nano Lett.* **15**, 6261–6266 (2015).
- [6] A. I. Kuznetsov, A. E. Miroshnichenko, M. L. Brongersma, Y. S. Kivshar, and B. Luk'yanchuk, *Science* **354**, aag2472 (2016).
- [7] P. Genevet, F. Capasso, F. Aieta, M. Khorasaninejad, and R. Devlin, *Optica* **4**, 139–152 (2017).
- [8] P. Lalanne, and P. Chavel, *Laser Photonics Rev.* **11**, 1600295 (2017).
- [9] D. Neshev, and I. Aharonovich, *Light Sci. Appl.* **7**, 58 (2018).
- [10] S. M. Kamali, E. Arbabi, A. Arbabi, and A. Faraon, *Nanophotonics* **7**, 1041–1068 (2018).
- [11] H. Liang, A. Martins, B.-H. V. Borges, J. Zhou, E. R. Martins, J. Li, and T. F. Krauss, *Optica* **6**, 1461–1470 (2019).
- [12] D. Lin, P. Fan, E. Hasman, and M. L. Brongersma, *Science* **345**, 298–302 (2014).
- [13] S. Vo, D. Fattal, W. V. Sorin, Z. Peng, T. Tran, M. Fiorentino, and R. G. Beausoleil, *IEEE Photonics Technol. Lett.* **26**, 1375–1378 (2014).
- [14] M. Khorasaninejad, W. T. Chen, R. C. Devlin, J. Oh, A. Y. Zhu, and F. Capasso, *Science* **352**, 1190–1194 (2016).
- [15] M.-S. L. Lee, P. Lalanne, J.-C. Rodier, and E. Cambril, *Opt. Lett.* **25**, 1690–1692 (2000).
- [16] A. Arbabi, Y. Horie, A. J. Ball, M. Bagheri, and A. Faraon, *Nat. Commun.* **6**, 1–6 (2015).
- [17] A. Arbabi, E. Arbabi, S. M. Kamali, Y. Horie, S. Han, and A. Faraon, *Nat. Commun.* **7**, 1–9 (2016).

- [18] A. Arbabi, Y. Horie, M. Bagheri, and A. Faraon, *Nat. Nanotechnol.* **10**, 937–943 (2015).
- [19] P. Lalanne, *J. Opt. Soc. Am. A* **16**, 2517–2520 (1999).
- [20] I. Staude, A. E. Miroshnichenko, M. Decker, N. T. Fofang, S. Liu, E. Gonzales, J. Dominguez, T. S. Luk, D. N. Neshev, I. Brener, and Y. Kivshar, *ACS Nano* **7**, 7824–7832 (2013).
- [21] M. Kerker, D. S. Wang, and C. L. Giles, *J. Opt. Soc. Am.* **73**, 765–767 (1983).
- [22] A. Rahimzadegan, D. Arslan, D. Dams, A. Groner, X. Garcia-Santiago, R. Alaei, I. Fernandez-Corbaton, T. Pertsch, I. Staude, and C. Rockstuhl, *Nanophotonics* **9**, 75–82 (2019).
- [23] I. Staude, T. Pertsch, and Y. S. Kivshar, *ACS Photonics* **6**, 802–814 (2019).
- [24] S. Kruk, and Y. Kivshar, in: *Dielectr. Metamaterials*, I. Brener, S. Liu, I. Staude, J. Valentine, and C. Holloway (eds.): (Woodhead Publishing, 2020), pp. 145–174.
- [25] A. J. Ollanik, J. A. Smith, M. J. Belue, and M. D. Escarra, *ACS Photonics* **5**, 1351–1358 (2018).
- [26] S. Li, X. Xu, R. M. Veetil, V. Valuckas, and A. I. Kuznetsov, *Science* **364**, 1087–1090 (2019).
- [27] H. Cai, S. Srinivasan, D. A. Czaplowski, A. B. F. Martinson, D. J. Gosztola, L. Stan, T. Loeffler, S. K. R. S. Sankaranarayanan, and D. López, *Npj Comput. Mater.* **6**, 1–8 (2020).
- [28] W. Zhao, H. Jiang, B. Liu, J. Song, Y. Jiang, C. Tang, and J. Li, *Sci. Rep.* **6**, 1–7 (2016).
- [29] J. P. Hugonin, and P. Lalanne, *Inst. d’Optique* (2005).
- [30] E. Popov, and M. Nevière, *J. Opt. Soc. Am. A* **18**, 2886–2894 (2001).
- [31] C. Gigli, P. Chavel, and P. Lalanne, in: *Proc. SPIE 11290, High Contrast Metastructures IX*, 112900U: (2020).
- [32] D. Arslan, K. E. Chong, A. E. Miroshnichenko, D. Choi, D. N. Neshev, T. Pertsch, Y. S. Kivshar, and I. Staude, *J. Phys. D: Appl. Phys.* **50**, 1–8 (2017).
- [33] S. Astilean, P. Lalanne, P. Chavel, E. Cambriil, and H. Launois, *Opt. Lett.* **23**, 552–554 (1998).
- [34] M. Oliva, T. Harzendorf, D. Michaelis, U. D. Zeitner, and A. Tünnermann, *Opt. Express* **19**, 14735–14745 (2011).
- [35] S. Person, M. Jain, Z. Lapin, J. J. Sáenz, G. Wicks, and L. Novotny, *Nano Lett.* **13**, 1806–1809 (2013).
- [36] Y. H. Fu, A. I. Kuznetsov, A. E. Miroshnichenko, Y. F. Yu, and B. Luk’yanchuk, *Nat. Commun.* **4**, 1–6 (2013).
- [37] M.-S. L. Lee, P. Legagneux, P. Lalanne, J.-C. Rodier, P. Gallais, C. Germain, and J. Rollin, *Opt. Eng.* **43**, 2583–2588 (2004).
- [38] J. Valentine, S. Zhang, T. Zentgraf, E. Ulin-Avila, D. A. Genov, G. Bartal, and X. Zhang, *Nature* **455**, 376–379 (2008).
- [39] J. Yang, C. Sauvan, H. T. Liu, and P. Lalanne, *Phys. Rev. Lett.* **107**, 1–4 (2011).
- [40] W. T. Chen, K. Y. Yang, C. M. Wang, Y. W. Huang, G. Sun, I. Da Chiang, C. Y. Liao, W. L. Hsu, H. T. Lin, S. Sun, L. Zhou, A. Q. Liu, and D. P. Tsai, *Nano Lett.* **14**, 225–230 (2014).